


 CrossMark  
click for updates

Cite this: DOI: 10.1039/c6ce00890a

# Solid-state and solution photoluminescence of platinum(II) complexes with 4'-substituted terpyridine ligands – structural, spectroscopic and electrochemical studies†

 A. Maroń,<sup>\*a</sup> A. Szlapa,<sup>b</sup> K. Czerwińska,<sup>a</sup> J. G. Matecki,<sup>a</sup> S. Krompiec<sup>b</sup> and B. Machura<sup>a</sup>

Platinum(II) complexes with the formula [PtCl(L)]CF<sub>3</sub>O<sub>3</sub>S (where L = 4'-(4-chlorophenyl)-2,2':6',2''-terpyridine (L<sub>1</sub>), 4'-(4-bromophenyl)-2,2':6',2''-terpyridine (L<sub>2</sub>), and 4'-(benzothiophene-2-yl)-2,2':6',2''-terpyridine (L<sub>3</sub>)) were synthesized from precursor [Pt(PhCN)<sub>2</sub>Cl<sub>2</sub>] and characterized by FT-IR, NMR, UV-vis spectroscopy, X-ray crystallography and electrochemical studies. The emission properties of the coordination compounds were studied in solution and in the solid state at ambient temperature and in methanol: ethanol frozen glass matrices at 77 K. The quantum yields of fluorescence, lifetimes and the nature of the excited states were described on the basis of the molecular properties of the compounds. To elucidate the structural, spectroscopic and bonding properties of the obtained compounds, calculations at the DFT level were undertaken. Coordination compounds are emissive in both solution and solid states. Emission energies and the character of excited states in solution are governed by the donor-acceptor properties of the 4' substituent of the terpyridine core. The emission properties in the solid state are attributed to the aggregation induced phenomenon. Moreover, the compounds [PtCl(L<sub>1</sub>)]CF<sub>3</sub>O<sub>3</sub>S and [PtCl(L<sub>2</sub>)]CF<sub>3</sub>O<sub>3</sub>S display a bathochromic shifted emission corresponding to J-aggregation (head-to-head Pt...Pt interactions), while in the case of compound [PtCl(L<sub>3</sub>)]CF<sub>3</sub>O<sub>3</sub>S a hypsochromic shifted emission compared to that in solution is characteristic of the H-aggregation process (head-to-tail Pt...π interaction). The coordination compounds display a strong rigidochromic effect with decay times changing from the ps/ns scale at ambient conditions to the μs domain in frozen glass matrices.

 Received 18th April 2016,  
Accepted 28th May 2016

DOI: 10.1039/c6ce00890a

[www.rsc.org/crystengcomm](http://www.rsc.org/crystengcomm)

## Introduction

Platinum(II) coordination compounds as luminophores are known for their possible applications in OLEDs,<sup>1–3</sup> non-linear

optics,<sup>4–6</sup> solar energy conversion<sup>7,8</sup> and also luminescence sensing materials.<sup>9</sup> The preferred properties are usually connected with long-lived room-temperature emission from triplet metal-to-ligand charge transfer (<sup>3</sup>MLCT) states observed for platinum(II) compounds. However, the terpyridine platinum(II) coordination compounds display weak photoluminescence properties in solution at room temperature due to the thermally accessible triplet metal-centered (<sup>3</sup>MC) state.<sup>10</sup> Through electron-withdrawing or electron-donating substituents on the 4'-position of the terpyridine core it is possible to increase the energy barrier between the <sup>3</sup>MLCT and the <sup>3</sup>MC states and prevent thermal deactivation.<sup>11</sup> Electron-withdrawing substituents (such as cyano and methylsulfonyl groups) decrease the energy of the <sup>3</sup>MLCT state; however, electron-donating groups (such as thioether or dimethylamino substituents) cause the appearance of a triplet intraligand charge transfer (<sup>3</sup>ILCT) state similar in energy to the <sup>3</sup>MLCT state, thus the emissive excited state is mixed <sup>3</sup>MLCT/<sup>3</sup>ILCT/<sup>3</sup>LC in character. However, relatively less known are the coordination platinum(II) compounds with

<sup>a</sup> Department of Crystallography, Institute of Chemistry, University of Silesia, 9th Szkolna St, 40-006 Katowice, Poland. E-mail: ank806@wp.pl

<sup>b</sup> Department of Inorganic, Organometallic Chemistry and Catalysis, Institute of Chemistry, University of Silesia, 9th Szkolna St, 40-006 Katowice, Poland

† Electronic supplementary information (ESI) available: FT-IR and NMR spectra of compounds, hydrogen bond in coordination compounds; stacking interactions in coordination compounds; composition of selected LUMOs and HOMOs of [PtCl(L<sub>1</sub>)]<sup>+</sup> and [PtCl(L<sub>2</sub>)]<sup>+</sup> cations; selected calculated transitions for coordination compounds; 2D fingerprint plots, coordination cations, Hirshfeld surfaces and percentage contributions to the surface area for the various close intermolecular contacts for molecules of compounds; density of states diagrams calculated for cationic forms of compounds; excitation and emission spectra in the form normalized intensity vs. wavelength of compounds; excitation and emission spectra with decay curves for compounds; comparison of emission spectra of compounds at different conditions. CIF files giving crystallographic data for complexes (1)–(3) CCDC 1033725, 1033726 and 1039074. For ESI and crystallographic data in CIF or other electronic format see DOI: 10.1039/c6ce00890a

terpyridines functionalized by substituted aryl groups or heterocycles and need further careful studies especially on the fields of impact of supramolecular architecture on solid-phase emission.

Coordination compounds of platinum(II) usually display enhanced solid state photoluminescence properties.<sup>12,13</sup> This phenomenon is connected with stacking intermolecular interactions. The square-planar geometry of d<sup>8</sup> Pt(II) compounds facilitates aggregation through attractive Pt–Pt and ligand–ligand interactions, which allows bi-molecular states (B–M) in the ground state or in the excited state.<sup>14</sup> Thus, compared to d<sup>6</sup> octahedral coordination compounds of iridium(III) or ruthenium(II), the platinum(II) compounds show an advantage due to the emission of broad visible light and possible generation of white light with a single dopant in luminescent materials. The arrangement of the stacking interaction in [Pt(4'-R-terpy)Cl]<sup>+</sup> additionally depends on the nature of the counter ions, which determines the solid-state colours and luminescence.<sup>9</sup>

In this report, we present a study on the synthesis and the structural, photophysical and electrochemical properties of platinum(II) chloride compounds with the formula [PtCl(L)]CF<sub>3</sub>O<sub>3</sub>S (where L = 4'-(4-chlorophenyl)-2,2':6',2''-terpyridine (L<sub>1</sub>), 4'-(4-bromophenyl)-2,2':6',2''-terpyridine (L<sub>2</sub>), and 4'-(benzothiophene-2-yl)-2,2':6',2''-terpyridine (L<sub>3</sub>)). The electronic structure is discussed on the basis of DFT calculations and used to interpret the luminescence properties of the compounds. The crystal and molecular structures were determined by X-ray crystallography. The spectroscopic properties were obtained using IR, UV-vis and NMR spectroscopy. The luminescence of compounds was studied at ambient temperature in solution and in the solid state. The solid state emission properties were correlated with the analysis of the Pt⋯Pt, π⋯π, Pt⋯π, Cl⋯π stacking interactions. The rigidochromic effect was examined to demonstrate the radiationless deactivation *via* the <sup>3</sup>MC state. The quantum yield and lifetime measurements were recorded to discuss the characteristics of the excited states.

## Experimental

### Materials and methods

All reagents used for the syntheses of the coordination compounds are commercially available and were used without further purification. The [Pt(PhCN)<sub>2</sub>Cl<sub>2</sub>] starting compound was obtained from Strem Chemicals Inc. The ligands, 4'-(4-chlorophenyl)-2,2':6',2''-terpyridine (L<sub>1</sub>), 4'-(4-bromophenyl)-2,2':6',2''-terpyridine (L<sub>2</sub>), and 4'-(benzothiophene-2-yl)-2,2':6',2''-terpyridine (L<sub>3</sub>), were synthesized according to procedures described previously in the literature.<sup>15–17</sup>

Infrared spectra were recorded on a Nicolet iS5 FT-IR spectrophotometer in the range 4000–400 cm<sup>-1</sup> using KBr pellets. Electronic absorption spectra were measured on a Nicolet iS50 UV-VIS-NIR spectrophotometer in the range of 900–180 nm in acetonitrile solution. The solid state (reflectance)

spectra were recorded for powder samples with the use of a 60 mm Spectralon® integrating sphere. The <sup>1</sup>H and <sup>13</sup>C NMR spectra were obtained at room temperature in CDCl<sub>3</sub> using a Bruker 500 MHz spectrometer. Elemental analyses (C, H, N) were performed on a Perkin-Elmer CHN-2400 analyzer.

Photoluminescence spectra were measured on an FLS-980 spectrophotometer. The room-temperature spectra were prepared in acetonitrile solution and in the solid state (powder). Low-temperature emission spectra were measured in an EtOH:MeOH mixture (4:1) frozen-glass matrix at the temperature of liquid nitrogen with a Dewar assembly. Quantum yields of optically diluted (0.05 < OD < 0.1) solutions and powders were measured with an integrating sphere using solvent (for solution samples) or Spectralon® reflectance standard (for powdered samples) as blanks. Time-resolved measurements were carried out at room temperature using the time correlated single photon counting method (TCSPC) on an FLS-980 spectrophotometer. The excitation wavelength was obtained using a set of picosecond pulsed diodes (EPLD-340 nm, EPL-375 nm) with a 500 ns pulse period as a light source and a PMT+500 nm (Hamamatsu, R928P) in a cooled housing was used as a detector. The system was aligned at the emission wavelengths. Additionally for the analysis of fluorescence decay, an instrument response function (IRF) was obtained. The IRF contains the information about the time response of the overall optical and electronic system. The IRF was designed using Ludox solution as a standard at excitation wavelengths.

Cyclic voltammetry (CV) and differential pulse voltammetry (DPV) measurements were carried out on an Autolab potentiostat (Eco Chemie). A three-electrode one-compartment cell was used to contain the solution of coordination compounds and supporting electrolyte in acetonitrile. Deaeration of the solution was achieved by bubbling argon through the solution for about 10 min before measurement. The compound and supporting electrolyte (n-Bu<sub>4</sub>NPF<sub>6</sub>) concentrations were 5 × 10<sup>-6</sup> mol dm<sup>-3</sup> and 0.02 mol dm<sup>-3</sup>, respectively. The scan rate was 0.1 V s<sup>-1</sup>. A glassy carbon disk working electrode (3 mm diam.) and a Ag/Ag<sup>+</sup> reference electrode were used. A ferrocene/ferrocenium (Fe/Fe<sup>+</sup>) electrode was added as an internal standard (the original data reported *vs.* Ag/Ag<sup>+</sup> have been converted using  $E_{(Fe/Fe^+)} = E_{(Ag/Ag^+)} - 0.5$  V to obtain the potential measured against Fe/Fe<sup>+</sup>). The energy of the HOMO and LUMO orbitals of the compounds was obtained from cyclic voltammograms using the following equations:  $E_{HOMO} = -5.1 - E_{ox}$ ,  $E_{LUMO} = -5.1 - E_{red}$ . All electrochemical experiments were carried out under ambient conditions.

### Synthetic procedure

A suspension of [Pt(PhCN)<sub>2</sub>Cl<sub>2</sub>] (0.10 g, 0.21 mmol) in acetonitrile (10 mL) was treated with an equimolar amount of Ag(CF<sub>3</sub>O<sub>3</sub>S) (0.054 g, 0.21 mmol) dissolved in acetonitrile (5 mL). The reaction mixture was heated under reflux for 16 h in the dark, the AgCl precipitate was removed by filtration

and one equivalent of ligand was added to the filtrate. The reaction mixture was heated in a solvothermal reactor under atmospheric pressure for an additional 24 h and then gradually cooled for another 24 h. Crystals suitable for X-ray analysis were obtained directly from the reaction mixtures.

(1) [PtCl(L<sub>1</sub>)]CF<sub>3</sub>O<sub>3</sub>S: yield 70%. C<sub>21</sub>H<sub>14</sub>Cl<sub>2</sub>N<sub>3</sub>Pt, CF<sub>3</sub>O<sub>3</sub>S. Anal. calc: C 36.53%, H 1.95%, N 5.81%. Anal. found: C 36.45%, H 1.98%, N 5.78%.

IR (KBr; cm<sup>-1</sup>): 3082 ν<sub>(ArH)</sub>; 1610, 1554 ν<sub>(C=N, C=C)</sub>; 1480, 1397 δ<sub>(C-CH out of the plane)</sub>; 1265 ν<sub>(C-N)</sub>; 1149, 1027 δ<sub>(C-CH in the plane)</sub>; 833, 779, 751, 717 δ<sub>(C-C out of the plane)</sub>; 636 δ<sub>(C-C in the plane)</sub>.

<sup>1</sup>H NMR (400 MHz, DMSO) δ 8.92 (s, 2H), 8.88 (d, *J* = 5.3 Hz, 2H), 8.75 (t, *J* = 11.4 Hz, 2H), 8.54–8.43 (m, 2H), 8.18 (t, *J* = 10.3 Hz, 2H), 7.96–7.87 (m, 2H), 7.75 (t, *J* = 9.0 Hz, 2H).

<sup>13</sup>C NMR (126 MHz, DMSO) δ 158.52, 154.92, 151.76, 143.02, 135.91, 133.65, 130.14, 130.00, 129.66, 126.45, 121.83.

UV-vis (ACN, nm (ε)): 404.5 (36 000), 385.0 (30 400), 352.4 (34 800), 333.6 (107 800), 307.3 (120 400), 281.8 (155 800), 260.1 (156 200); (solid, nm (Abs)): 512.6 (0.929), 426.4 (1.055), 346.6 (0.923), 252.5 (0.751).

(2) [PtCl(L<sub>2</sub>)]OTf: yield 70%. C<sub>21</sub>H<sub>14</sub>ClBrN<sub>3</sub>Pt, CF<sub>3</sub>O<sub>3</sub>S. Anal. calc: C 34.41%, H 1.84%, N 5.47%. Anal. found: C 34.50%, H 1.80%, N 5.43%.

IR (KBr; cm<sup>-1</sup>): 3082 ν<sub>(ArH)</sub>; 1611, 1587 ν<sub>(C=N, C=C)</sub>; 1479, 1414 δ<sub>(C-CH out of the plane)</sub>; 1247, 1224 ν<sub>(C-N)</sub>; 1149, 1029 δ<sub>(C-CH in the plane)</sub>; 829, 780, δ<sub>(C-C out of the plane)</sub>; 636 δ<sub>(C-C in the plane)</sub>.

<sup>1</sup>H NMR (400 MHz, DMSO) δ 8.79 (d, *J* = 9.4 Hz, 2H), 8.61 (dd, *J* = 28.4, 6.3 Hz, 4H), 8.39 (t, *J* = 7.7 Hz, 2H), 8.04 (d, *J* = 8.5 Hz, 2H), 7.87 (d, *J* = 8.3 Hz, 2H), 7.84–7.75 (m, 2H).

<sup>13</sup>C NMR (126 MHz, DMSO) δ 158.16, 154.62, 151.61, 151.50, 142.92, 133.87, 132.89, 130.20, 129.67, 126.48, 126.28, 122.49, 121.43, 119.83.

UV-vis (ACN, nm, (ε)): 404.2 (20 800), 384.6 (17 000), 331.9 (64 800), 308.6 (68 000), 281.6 (91 000), 260.2 (88 800); (solid, nm (Abs)): 513.6 (0.825), 422.8 (1.018), 343.7 (0.889), 252.8 (0.701).

(3) [PtCl(L<sub>3</sub>)]OTf: yield 78%. C<sub>23</sub>H<sub>15</sub>ClN<sub>3</sub>PtS, CF<sub>3</sub>O<sub>3</sub>S. Anal. calc: C 38.69%, H 2.03%, N 5.64%. Anal. found: C 38.75%, H 2.12%, N 5.58%.

IR (KBr; cm<sup>-1</sup>): 3059 ν<sub>(ArH)</sub>; 1611, 1554 ν<sub>(C=N, C=C)</sub>; 1478, 1429 δ<sub>(C-CH out of the plane)</sub>; 1256, 1223 ν<sub>(C-N)</sub>; 1157, 1029 δ<sub>(C-CH in the plane)</sub>; 782, 754 δ<sub>(C-C out of the plane)</sub>; 637 δ<sub>(C-C in the plane)</sub>.

<sup>1</sup>H NMR (400 MHz, DMSO) δ 8.63 (s, 2H), 8.43 (s, 2H), 8.35 (t, *J* = 7.5 Hz, 2H), 8.03 (d, *J* = 7.8 Hz, 2H), 7.90 (d, *J* = 7.6 Hz, 2H), 7.77 (s, 1H), 7.50 (dt, *J* = 14.7, 7.1 Hz, 4H).

<sup>13</sup>C NMR (126 MHz, DMSO) δ 157.87, 154.56, 151.48, 146.37, 142.71, 141.11, 139.76, 138.29, 129.65, 128.39, 127.81, 126.45, 126.18, 125.71, 123.33, 122.48, 120.07.

UV-vis (ACN, nm, (ε)): 423.3 (48 000), 401.0 (34 200), 323.4 (53 600), 283.4 (81 800), 255.0 (65 600), 228.2 (67 400), 207.5 (88 000); (solid, nm (Abs)): 592.1 (0.774), 546.6 (0.889), 473.8 (1.135), 444.1 (1.147), 419.2 (1.140), 356.3 (1.059), 272.8 (0.943).

FT-IR and NMR spectra for compounds (1)–(3) are collected in the ESI†

## Crystallography

Crystals of the coordination compounds (1)–(3) were mounted in turn on a Gemini A Ultra Oxford Diffraction automatic diffractometer equipped with a CCD detector and used for data collection. X-ray intensity data were collected with graphite monochromated MoK<sub>α</sub> radiation (λ = 0.71073 Å) at a temperature of 295(2) K with ω scan mode. Ewald sphere reflections were collected up to 2θ = 50.10°. Details concerning crystal data and refinement are gathered in Table 1. The unit cell determination and data integration were carried out using the CrysAlis package<sup>18</sup> of Oxford Diffraction. Lorentz, polarization and empirical absorption corrections using spherical harmonics implemented in SCALE3 ABSPACK scaling algorithm were applied. The structures were solved by the Patterson method and subsequently completed by difference Fourier recycling. All the non-hydrogen atoms were refined anisotropically using full-matrix least-squares techniques. All hydrogen atoms were positioned in geometrically idealized positions and were allowed to ride on their parent atoms with *U*<sub>iso</sub>(H) = 1.2*U*<sub>eq</sub>. The Olex2,<sup>19</sup> SHELXS, and SHELXL<sup>20</sup> programs were used for all the calculations. Atomic scattering factors were incorporated into the computer programs.

## Quantum calculations

The calculations were carried out using the Gaussian09<sup>21</sup> program. Molecular geometries of the singlet ground state of the cationic forms of the platinum(II) compounds were optimized in acetonitrile solutions with the Polarizable Continuum Model (PCM) model<sup>22</sup> at the B3LYP level of theory.<sup>23</sup> For each compound a frequency calculation was carried out, verifying that the optimized molecular structure obtained corresponds to a local energy minimum; thus only positive frequencies were found. The Pt-mDZP basis set<sup>24</sup> was used to describe the platinum atom and the basis set used for the lighter atoms (Cl, N, B, C, H) was 6-31G\*\*. The TD-DFT method<sup>25–27</sup> was employed to calculate the electronic absorption spectra in the PCM<sup>22</sup> using acetonitrile as a solvent.

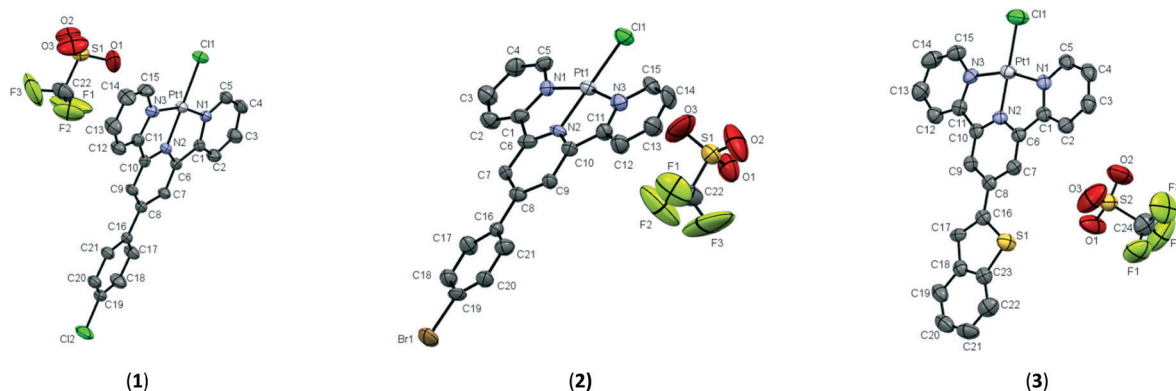
## Results and discussion

### Crystal structure

Syntheses of platinum(II) coordination compounds were conducted with [PtCl<sub>2</sub>(NCPH)<sub>2</sub>] as a precursor using a modification of Dhara's method.<sup>28</sup> The coordination compounds crystallize in the monoclinic space groups *P*<sub>2</sub><sub>1</sub>/*c* and *P*<sub>2</sub><sub>1</sub>/*n* and their structures, as ORTEP representations with labeling schemes, are shown in Fig. 1 while selected experimental and calculated bond distances and angles are given in Table 2 (see also Tables S1 and S2 in the ESI†). The bond lengths and angles calculated by DFT method for cationic forms of the coordination compounds are in agreement with experimental values as can be seen from the data collected in Table 2.

**Table 1** Crystallographic data for complexes (1)–(3)

	(1)	(2)	(3)
Empirical formula	C <sub>21</sub> H <sub>14</sub> Cl <sub>2</sub> N <sub>3</sub> Pt, CF <sub>3</sub> O <sub>3</sub> S	C <sub>21</sub> H <sub>14</sub> ClBrN <sub>3</sub> Pt, CF <sub>3</sub> O <sub>3</sub> S	C <sub>23</sub> H <sub>15</sub> ClN <sub>3</sub> PtS, CF <sub>3</sub> O <sub>3</sub> S
Formula weight	723.41	767.87	745.05
Temperature [K]	295(2)	295(2)	295(2)
Crystal system	Monoclinic	Monoclinic	Monoclinic
Space group	<i>P</i> 2 <sub>1</sub> / <i>c</i>	<i>P</i> 2 <sub>1</sub> / <i>c</i>	<i>P</i> 2 <sub>1</sub> / <i>n</i>
Unit cell dimensions			
<i>a</i> [Å]	7.3698(3)	7.4264(4)	16.2788(13)
<i>b</i> [Å]	21.6379(12)	21.7744(14)	7.0245(7)
<i>c</i> [Å]	14.5584(7)	14.5258(8)	21.716(2)
$\alpha$ [°]	90	90	90
$\beta$ [°]	102.509(4)	102.970(5)	98.966(7)
$\gamma$ [°]	90	90	90
Volume [Å <sup>3</sup> ]	2266.47(19)	2289.0(2)	2452.9(4)
<i>Z</i>	4	4	4
Calculated density [Mg m <sup>-3</sup> ]	2.120	2.228	2.018
Absorption coefficient [mm <sup>-1</sup> ]	6.576	8.140	6.056
<i>F</i> (000)	1384	1456	1432
Crystal dimensions [mm]	0.31 × 0.13 × 0.05	0.39 × 0.11 × 0.04	0.12 × 0.10 × 0.04
$\theta$ range for data collection [°]	3.44–25.05	3.55–25.05	3.36–25.05
Index ranges	−8 ≤ <i>h</i> ≤ 7 −25 ≤ <i>k</i> ≤ 25 −15 ≤ <i>l</i> ≤ 17	−8 ≤ <i>h</i> ≤ 7 −25 ≤ <i>k</i> ≤ 23 −17 ≤ <i>l</i> ≤ 16	−19 ≤ <i>h</i> ≤ 19 −8 ≤ <i>k</i> ≤ 8 −20 ≤ <i>l</i> ≤ 25
Reflections collected	12 767	11 339	14 019
Independent reflections	4006 [ <i>R</i> (int) = 0.0328, <i>R</i> <sub>σ</sub> = 0.0344]	4039 [ <i>R</i> (int) = 0.0679, <i>R</i> <sub>σ</sub> = 0.0682]	4335 [ <i>R</i> (int) = 0.0367, <i>R</i> <sub>σ</sub> = 0.0354]
Data/restraints/parameters	4006/0/316	4039/0/316	4335/0/334
Goodness of fit on <i>F</i> <sup>2</sup>	1.034	1.039	1.041
Final <i>R</i> indices [ <i>I</i> > 2σ( <i>I</i> )]	<i>R</i> <sub>1</sub> = 0.0272 <i>wR</i> <sub>2</sub> = 0.0583	<i>R</i> <sub>1</sub> = 0.0545 <i>wR</i> <sub>2</sub> = 0.1342	<i>R</i> <sub>1</sub> = 0.0288 <i>wR</i> <sub>2</sub> = 0.0631
<i>R</i> indices (all data)	<i>R</i> <sub>1</sub> = 0.0374 <i>wR</i> <sub>2</sub> = 0.0614	<i>R</i> <sub>1</sub> = 0.0713 <i>wR</i> <sub>2</sub> = 0.1448	<i>R</i> <sub>1</sub> = 0.0403 <i>wR</i> <sub>2</sub> = 0.0673
Largest diff. peak and hole	0.760/−0.621	2.938/−1.901	0.689/−0.602

**Fig. 1** ORTEP drawing of complexes (1)–(3) with 50% probability displacement ellipsoids.**Table 2** Selected experimental and calculated bond lengths [Å] and angles [°] for complexes (1)–(3)

	(1)		(2)		(3)	
	Exp	Calc	Exp	Calc	Exp	Calc
Bond length [Å]						
Pt(1)–N(1)	2.016(4)	2.07	2.017(8)	2.07	2.015(4)	2.07
Pt(1)–N(2)	1.930(3)	1.98	1.931(6)	1.98	1.931(3)	1.98
Pt(1)–N(3)	2.025(4)	2.07	2.019(8)	2.07	2.018(4)	2.07
Pt(1)–Cl(1)	2.2994(11)	2.40	2.299(2)	2.40	2.2961(14)	2.40
Angle [°]						
N(2)–Pt(1)–N(1)	80.88(15)	80.2	80.9(3)	80.2	81.11(15)	80.1
N(2)–Pt(1)–N(3)	81.05(15)	80.2	80.5(3)	80.2	81.19(15)	80.1
N(1)–Pt(1)–N(3)	161.92(14)	160.4	161.4(3)	160.4	162.25(15)	160.3
N(1)–Pt(1)–Cl(1)	99.06(10)	99.8	99.3(2)	99.8	98.57(11)	99.9
N(2)–Pt(1)–Cl(1)	179.61(12)	180.0	179.7(3)	180.0	179.12(12)	180.0
N(3)–Pt(1)–Cl(1)	99.01(11)	99.8	99.3(2)	99.8	99.14(11)	99.9

The platinum(II) metal center in the coordination cations adopts a distorted square-planar geometry due to the geometric constraints imposed by the terpyridyl ligand. The N–Pt–N angles deviate from the ideal 90° and 180° by about 10° and 19° (see Table 2), respectively, due to the steric demand of the terpyridine ligands. The geometries (bond lengths, angles) of the coordination sphere around the platinum ion are almost the same in each of the compounds: geometry indices  $\tau_4$  and  $\tau_4^{29,30}$  are respectively equal to 0.1309°, 0.0761° (1); 0.1340, 0.0773 (2) and 0.1321, 0.0798 (3). However, some differences are visible within the geometries of the terpy ligands. The coordinated terpyridine moieties are almost planar, with the dihedral angles between the central pyridine plane and the two lateral ones equal to 5.90° and 2.87° in (1), 5.87°, 3.11° in (2) and 4.22°, 1.27° in (3), whereas the 4' substituent planes are inclined to the central pyridine rings at 10.50°, 9.40° and 1.17° in (1)–(3), respectively.

The crystal packings of (1) and (2) show the stacking interactions between pairs of the coordination cations (Table S2† and Fig. 2),<sup>31</sup> with alternating intermolecular Pt···Pt distances of 3.57 Å. In the crystal structure of (3) the Pt···Pt interaction does not exist; instead a head-to-tail stacking creates a Pt– $\pi$  benzene ring interaction with a distance of 3.70 Å (see Table S2C† and Fig. 2). Examination of the packing diagrams reveals also that the structures of the coordination compounds exhibit  $\pi$ – $\pi$  interactions between aromatic terpyridine moiety rings; C–H··· $\pi$  and C–F··· $\pi$  ring<sup>32</sup> interactions occurred in compounds (1) and (2). Moreover, in the coordination compounds (1) and (2) the Pt–Cl··· $\pi$  ring interactions are visible with distances close to 3.8 Å. The various intermolecular interactions further confirmed by Hirshfeld surface analysis<sup>33–35</sup> (see Fig. S1 in the ESI†) affect the luminescence properties of these compounds, especially the presence of the interactions between the platinum centers in the structures of compounds (1) and (2) and in the case of compound (3) the planarity of 4'-(benzothiophene-2-yl)-2,2':6',2''-terpyridine.

## Electronic absorption and emission spectra

**Absorption spectra in solution and solid state.** Solution samples of the coordination compounds display well-shaped, wide charge transfer bands with maxima at 404 nm for (1), (2) and 423 nm for (3) on the absorption spectra. The energy of these absorption bands depends mostly on the  $\pi$ -donating ability of the substituent in the 4' position of the terpyridine moiety, increasing in the order  $L_1 < L_2 < L_3$ , which is additionally confirmed by DFT calculations. The participation of the substituent in the 4' position of the terpyridine core in the HOMO increases in the range (1) < (2) < (3) as one can see from the data collected in Table S3 in the ESI† where the compositions of the selected LUMOs and HOMOs of the coordination cations are presented and from the densities of states (DOS) diagrams (*cf.* Fig. S2†) calculated using the GaussSum program.<sup>36</sup> The transitions in this range (according to Table S4 in ESI†) can be assigned as H-1/H-2  $\rightarrow$  LUMO and

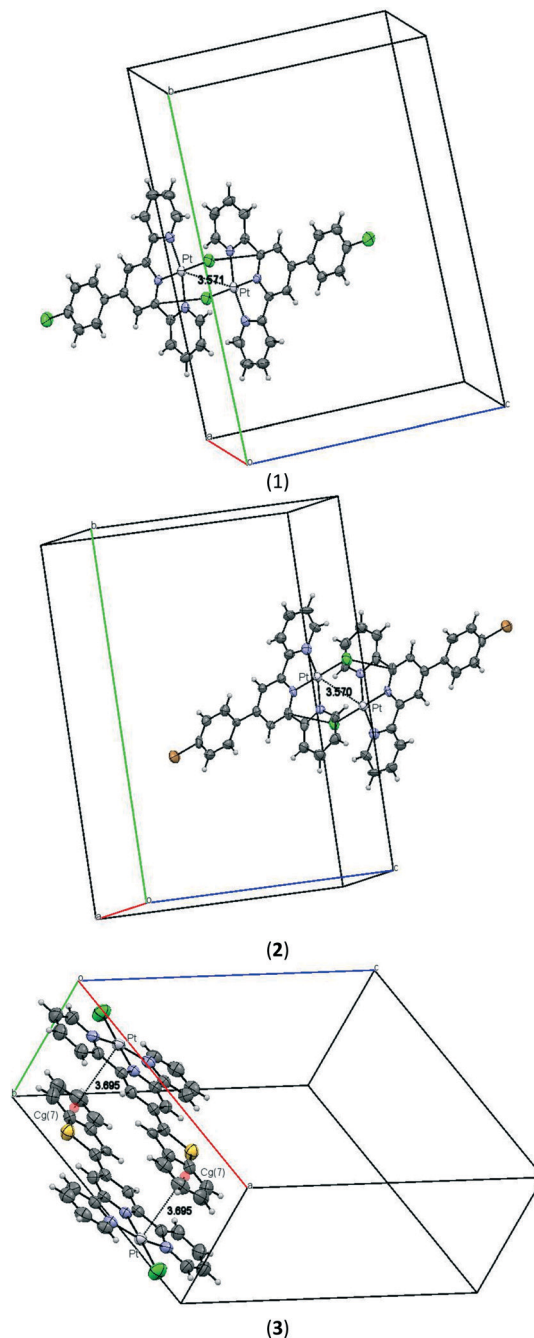


Fig. 2 Contact interactions in the crystal structures of (1)–(3).

can be characterized as mixed XLCT/MLCT in the case of (1) and (2) or ILCT in the case of benzothiophene-2-yl substituted compound (3).

Solid state absorption spectra are dominated by one or two bands, which are bathochromic shifted compared to solution-phase spectra. The ranges of these shifts are equal to 1278  $\text{cm}^{-1}$ , 1056  $\text{cm}^{-1}$ , and 1118  $\text{cm}^{-1}$  for compounds (1)–(3), respectively. Visible broadening of the solid state absorption spectra compared to the solution-phase spectra is characteristic of strong intermolecular coupling in the aggregates.<sup>37</sup> The experimental and calculated electronic

absorption spectra in solution are graphically compared with absorption spectra in the solid phase of the compounds in Fig. 3.

#### Emission spectra in solution, solid state and rigid matrix.

The excitation and emission spectra are presented in Fig. 4. The spectroscopic and electrochemical properties are listed in Table 3 (see also Fig. S3 and S4 in the ESI†).

Acetonitrile solutions of the compounds at ambient conditions display excitation bands at 368 nm, 432 nm (1), 366 nm (2), and 465 nm (3). Excitation of (1) and (2) in solution gives rise to one structureless emission band with a maximum at 518 and 528 nm, respectively, while excited compound (3) displays a structured emission band with maxima at 545 nm, 607 nm, and 668 nm (sh). Calculated transitions corresponding to excitation wavelengths are HOMO  $\rightarrow$  LUMO/L+1 according to Table S4† (italic lines). On this basis, it can be concluded that the orbital parentages of excited states in the case of (1) and (2) are mixed and the excitation has a partly  $d-\pi^*$ ,  $\pi_{(Cl)}-\pi^*_{(core)}$  and  $\pi_{(R)}-\pi^*_{(terpy)}$  character. However, for compound (3) the excited state has an ILCT character due to the greater ability of the benzothiophene-2-yl substituent to donate electrons to the terpy core than the 4-chloro/bromophenyl substituents. Efficient decreasing of the energy gap caused by the benzothiophene-2-yl substituent explains the significant bathochromic shift of the emission maxima in the case of (3) (see also ‘Electrochemical properties’ section). Compound (2) shows weaker luminescence properties ( $\Phi$  and  $\tau$ ) than compound (1) in solution due to the internal heavy atom effect observed when changing the chloro substituent to a bromo substituent. Compared with known  $[Pt(4'-X-T)Cl]^+$  (where X = CN, SO<sub>2</sub>Me, H, SMe, NMe<sub>2</sub>), an increase in quantum efficiency by an order of magnitude is observed.<sup>11</sup> Such an increase in the quantum efficiency is characteristic of platinum terpyridine compounds with electron-donating substituents<sup>38</sup> or polycyclic substituents<sup>39</sup> due to mixing of the <sup>3</sup>MLCT excited state with <sup>3</sup>ILCT and/or <sup>3</sup>LC states. However, the values of the decay times indicate thermal deactivation of the emissive excited states by <sup>3</sup>MC states, which was already observed earlier.<sup>9,40</sup>

A major feature of the studied compounds is the emission in the solid phase. All three compounds display a relatively long-lived emission ( $\sim$ 500–1000 ns) as powdered sam-

ples as a result of intermolecular interactions observed in the crystal arrangement of compounds (see ‘Crystal structure’ section). It is well known that enhanced properties ( $\Phi$  and  $\tau$ ) of emission in the solid state are usually attributed to the aggregation induced phenomenon.<sup>41</sup> The solid-state emission spectra of (1) and (2) at room temperature show structureless bands with the maxima largely bathochromic shifted with respect to the values reported for solutions (5080 cm<sup>-1</sup> (1), 4755 cm<sup>-1</sup> (2)) due to the head-to-head Pt $\cdots$ Pt interactions predisposed to the J-aggregation process. However, in the case of compound (3) the structured solid state emission band shows a hypsochromic shift compared to emission maxima in solution (2398 cm<sup>-1</sup>), which is associated with the head-to-tail Pt- $\pi$  stackings that allow the formation of H-aggregates (see Fig. 2 and S5 in the ESI†).

The rigidochromic effect was studied in methanol:ethanol frozen glass matrices at the temperature of liquid nitrogen to better understand the nature of the lowest emissive excited states. For all three compounds low-temperature emission spectra reveal a vibronic structure with three to four bands (see Table 3 and Fig. 4). It is well known that the vibronic shape of the emission spectra in a rigid matrix is typical of emission originating from both MLCT and ILCT states and a distinction between these states can be raised by the time-resolved spectra. Thus, the lifetime values at low temperature compared to those at ambient conditions, increasing from the nanosecond/picosecond scale in the case of ambient temperature to the microsecond domain at 77 K, indicate the elimination of the thermal deactivation process observed at ambient conditions. Moreover, a very similar range of emission, the decay times ( $\sim$ 20  $\mu$ s) and the slight hypsochromic shift of low-temperature spectra relative to the emission band at ambient conditions (equal to 226 cm<sup>-1</sup> and 592 cm<sup>-1</sup>) in the case of compounds (1) and (2) indicate the emission from the <sup>3</sup>MLCT excited state. However, the spectra of compound (3) are significantly bathochromic shifted (1225 cm<sup>-1</sup>), which allows the interpretation that the emission of (3) is connected with different excited states and should be considered as phosphorescence of <sup>3</sup>ILCT. The longest lifetime, about 60  $\mu$ s, additionally is in accordance with this study.

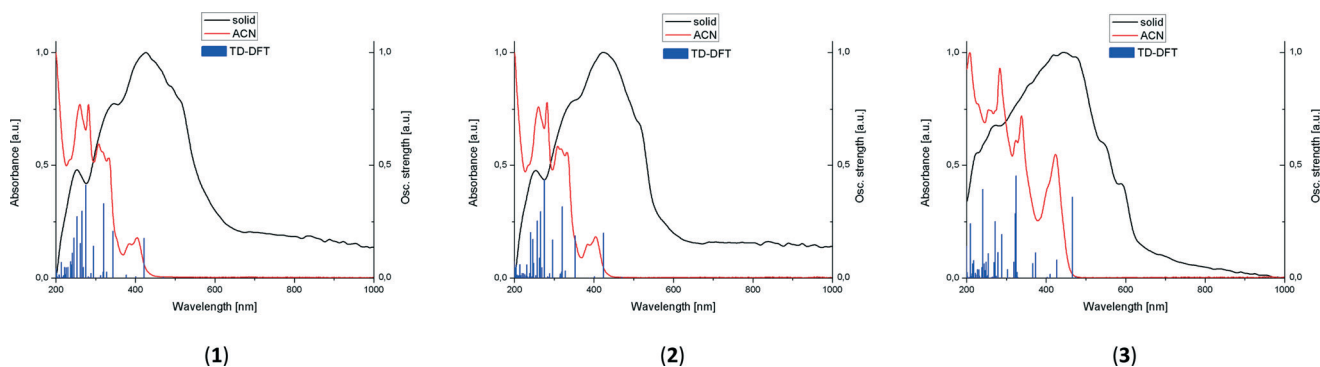
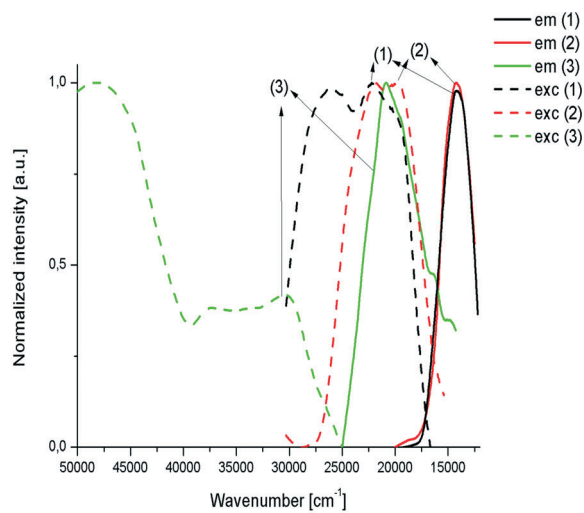
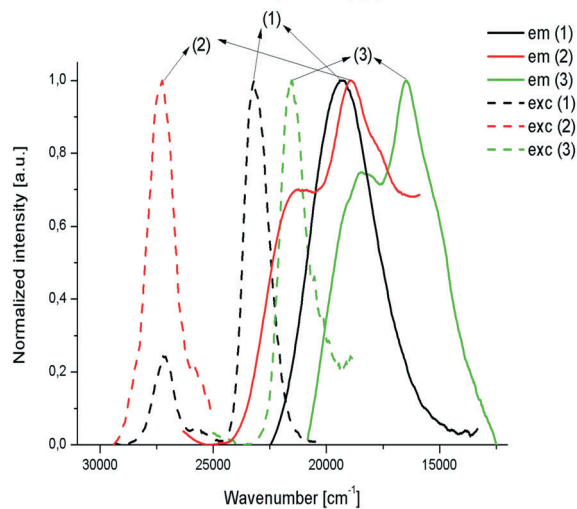


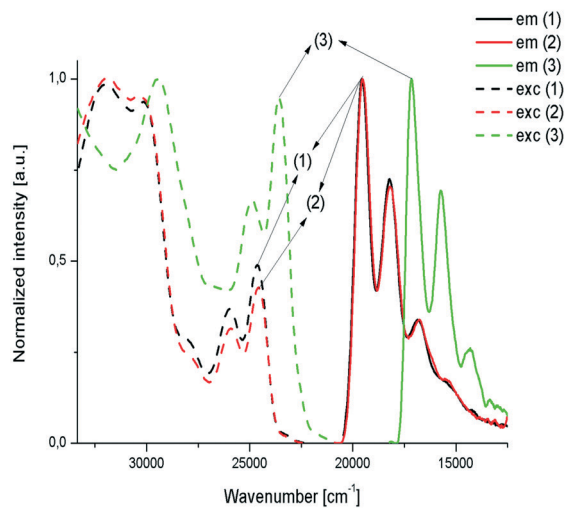
Fig. 3 Absorption spectra of complexes (1)–(3).



**Solid:**  $\lambda_{\text{exc}} = 20833 \text{ cm}^{-1}$  (480 nm) (1);  $20000 \text{ cm}^{-1}$  (500 nm) (2);  
 $30303 \text{ cm}^{-1}$  (330 nm) (3)



**ACN:**  $\lambda_{\text{exc}} = 23256 \text{ cm}^{-1}$  (430 nm) (1);  $27397 \text{ cm}^{-1}$  (365 nm) (2);  
 $21505 \text{ cm}^{-1}$  (465 nm) (3)



**77K:**  $\lambda_{\text{exc}} = 24691 \text{ cm}^{-1}$  (405 nm) (1);  $24691 \text{ cm}^{-1}$  (405 nm) (2);  
 $23529 \text{ cm}^{-1}$  (425 nm) (3)

Fig. 4 Excitation and emission spectra of complexes (1)–(3).

## Electrochemical properties

Cyclic voltammograms of the compounds are shown in Fig. 5. The spectroscopic and electrochemical data for coordination compounds (1)–(3) are listed in Table 3.

The examined platinum(II) coordination compounds exhibit a two-step ligand based reduction. The first reduction couple is quasi-reversible in nature as is consistent with the peak potential separations generally larger than the ideal Nernstian value of 59 mV for a one-electron transfer. The  $\Delta E$  values are 78.1 mV, 83.0 mV and 65.9 mV for compounds (1)–(3), respectively. The half-wave potentials of ligand based reduction are similar for compounds (1) and (2); however, for compound (3), due to the  $\pi$ -acidity differences of substituents in the 4' position of the terpy core, they have significantly a more positive value.

The oxidation peaks at 0.735 V (1), 0.817 V (2) and 1.061 V (3) are irreversible. The pulses in this range can be attributed to the oxidation of the metal center; however the increasing sharing of oxidation within substituents should be taken into account. The potentials of the oxidation process increased with the increasing sharing of ligand orbitals in HOMOs gradually from (1) to (3).

The energies of LUMO orbitals obtained from cyclic voltammograms of the compounds differ between  $-3.36 \text{ eV}$  and  $-3.88 \text{ eV}$ ; however, the energy of HOMOs are in the range from  $-5.84 \text{ eV}$  to  $-6.16 \text{ eV}$ . The decreasing tendency of the energy band gap characteristic of (3) is clearly visible from the electrochemical data and generally explains the lowering of the energy of emission observed in solutions of compounds (3) compared to (1) and (2). The electrochemically determined band gaps are in good agreement with the optical band gaps. Moreover, the electrochemical data indicate rather the significant stabilization of the energy of LUMOs than the destabilization of the energy of HOMOs, which practically means a greater impact of electron-accepting properties than the electron-donating effect of the substituent in the terpy core especially in the case of compound (3). Taking into account electrochemistry studies, the influences of the ligand substituents on the emission process of coordination compounds should be considered as both electron-donating and electron-withdrawing effects of the substituents in the 4' position of the terpy core. In the case of compound (3) with the benzothiophene-2-yl group present in the molecular structure, both electron-donating and electron-withdrawing effects have an impact on the emission properties and cause the efficient shift of emission compared to compounds (1) and (2).<sup>42</sup>

## Conclusions

Summarizing, by modification of Dhara's method triflate platinum(II) coordination compounds with 4'-substituted derivatives of 2,2':6',2''-terpyridine were synthesized. The compounds were studied by NMR, FT-IR, UV-vis spectroscopy and cyclic voltammetry. The molecular structures of the platinum(II) coordination compounds (1)–(3) have been

**Table 3** Spectroscopic and electrochemical properties of compounds (1)–(3)

	$\lambda_{\text{exc}}$ [nm] ( $\text{cm}^{-1}$ )			$\lambda_{\text{em}}$ [nm] ( $\text{cm}^{-1}$ )			$\tau$ [ns] ( $\Phi_{\text{em}}$ [%])		
	Solid	ACN	77 K	Solid	ACN	77 K	Solid	ACN	77 K
(1)	372 (26882), 479 (20877) <sup>a</sup>	368 (27174), 432 (23148) <sup>a</sup>	286 (34965), 310 (32258), 335 (29851), 356 (28090), 385 (25874), 407 (24570) <sup>a</sup>	703 (14225)	518 (19305)	512 (19531), <sup>a</sup> 550 (18182), 593 (16863), 649 (15408) (sh)	496.32 (6.32)	3.01 (6.21)	23693.0
(2)	450 (22222), 499 (20040) <sup>a</sup>	366 (27322)	314 (31847), 334 (29940), 386 (25907), 407 (24570) <sup>a</sup>	705 (14184)	528 (18939)	512 (19531), <sup>a</sup> 549 (18215), 595 (16807), 647 (15456) (sh)	821.80 (7.30)	2.02 (0.61)	23389.4
(3)	328 (30488)	465 (21505)	307 (32573), 339 (29498), 402 (24876), 424 (23585) <sup>a</sup>	482 (20747), <sup>a</sup> 505 (19802) (sh), 613 (16313) (sh)	545 (18349), 607 (16474), <sup>a</sup> 668 (14970) (sh)	584 (17123), <sup>a</sup> 636 (15723), 699 (14306) (sh)	1191.04 (1.12)	4.94 (2.01)	62434.3

	$\Delta E$ [ $\text{cm}^{-1}$ ]			$E_{\text{g}}^{\text{opt}}$ [eV]			CV				
	Solid	ACN	77 K	Solid	ACN	77 K	$E_{\text{ox}}$ [V]	$E_{\text{red}}$ [V] ( $\Delta E$ [mV])	$E_{\text{HOMO}}$ [eV]	$E_{\text{LUMO}}$ [eV]	$E_{\text{g}}^{\text{CV}}$ [eV]
(1)	6652	3843	5039	1.76	2.40	2.42	0.735	-1.741 (78.1), -2.463	-5.84	-3.36	2.48
(2)	5856	8383	5039	1.76	2.35	2.42	0.817	-1.718 (83.0), -2.167	-5.92	-3.38	2.54
(3)	9741	5031	6462	2.57	2.04	2.12	1.060	-1.219 (65.9), -2.410	-6.16	-3.88	2.28

<sup>a</sup> The most intensive band; sh – shoulder.

determined by X-ray diffraction studies on single crystals. The coordination compounds display both solid-state and solution-phase emission. The emission properties in the solid phase are attributed to the aggregation induced phenomenon. Solid-state emission of compounds (1) and (2) are significantly bathochromic shifted compared to solution-phase emission due to the J-aggregation process connected with head-to-head Pt···Pt interaction. However, the hypsochromic shift of solid-state emission in the case of compound (3) is attributed to the H-aggregation process *via* head-to-tail Pt– $\pi$  intermolecular interactions. The electrochemical properties of coordination compounds are in agreement with the optical properties in solution phase. On this basis, it can be concluded that the lowering of emission energy in the case of compound (3) compared to that in compounds (1) and (2) can be attributed to the decrease in the energy band gap

caused by substituent effect. The strong rigidochromic effect characteristic of coordination compounds indicates on the one hand that the thermal deactivation process *via* the <sup>3</sup>MC state occurs at ambient conditions and on the other hand proves the different character of the lowest emissive excited state in the case of coordination compounds (1) and (2) compared to coordination compound (3).

## Acknowledgements

The research was co-financed by the National Research and Development Center (NCBiR) under Grant ORGANOMET No: PBS2/A5/40/2014. Calculations have been carried out in Wroclaw Centre for Networking and Supercomputing (<http://www.wcss.wroc.pl>) under grant number 18.

## Notes and references

- 1 D. A. K. Vezzu, J. C. Deaton, J. S. Jones, L. Bartolotti, C. F. Harris, A. P. Marchetti, M. Kondakova, R. D. Pike and S. Huo, *Inorg. Chem.*, 2010, 49(11), 5107.
- 2 E. Turner, N. Bakken and J. Li, *Inorg. Chem.*, 2013, 52(13), 7344.
- 3 J. A. G. Williams, S. Develay, D. L. Rochester and L. Murphy, *Coord. Chem. Rev.*, 2008, 252, 2596.
- 4 R. Liu, A. Azenkeng, D. Zhouc, Y. Li, K. D. Glusac and W. Sun, *J. Phys. Chem. A*, 2013, 117, 1907.
- 5 B. Zhang, Y. Li, R. Liu, T. M. Pritchett, A. Azenkeng, A. Ugrinov, J. E. Haley, Z. Li, M. R. Hoffmann and W. Sun, *Chem. – Eur. J.*, 2012, 18, 4593.
- 6 W. Sun, B. Zhang, Y. Li, T. M. Pritchett, Z. Li and J. E. Haley, *Chem. Mater.*, 2010, 22, 6384.

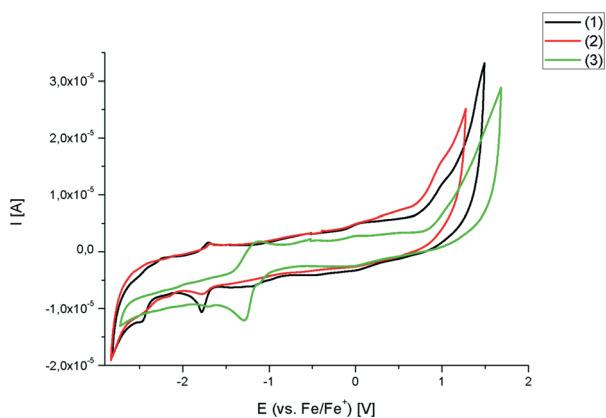


**Fig. 5** Cyclic voltammograms of compounds (1)–(3).

- 7 S. Suzuki, R. Sugimura, M. Kozaki, K. Keyaki, K. Nozaki, N. Ikeda, K. Akiyama and K. Okada, *J. Am. Chem. Soc.*, 2009, **131**, 10374.
- 8 J. E. McGarrah, Y.-J. Kim, M. Hissler and R. Eisenberg, *Inorg. Chem.*, 2001, **40**, 4510.
- 9 K. M.-C. Wong and V. W.-W. Yam, *Coord. Chem. Rev.*, 2007, **251**, 2477.
- 10 V. H. Houlding and V. M. Miskowski, *Coord. Chem. Rev.*, 1991, **111**, 145.
- 11 D. R. McMillin and J. J. Moore, *Coord. Chem. Rev.*, 2002, **229**, 113.
- 12 H. Imoto, S. Tanaka, T. Kato, S. Watase, K. Matsukawa, T. Yumura and K. Naka, *Organometallics*, 2016, **35**, 364; G. Y. Zheng and D. P. Rillema, *Inorg. Chem.*, 1998, **37**, 1392.
- 13 J. S. Field, L. P. Ledwaba, O. Q. Munro and D. R. McMillin, *CrystEngComm*, 2008, **10**, 740.
- 14 J. Kalinowski, V. Fattori, M. Cocchi and J. A. G. Williams, *Coord. Chem. Rev.*, 2011, **255**, 2401.
- 15 J. Wang and G. S. Hanan, *Synlett*, 2005, **8**, 1251.
- 16 A. N. Kharat, A. Bakhoda and S. Zamanian, *Polyhedron*, 2011, **30**, 1134.
- 17 E. C. Constable, E. L. Dunphy, C. E. Housecroft, M. Neuburger, S. Schaffner, F. Schaper and S. R. Batten, *Dalton Trans.*, 2007, 4323.
- 18 RED CrysAlis, *Oxford Diffraction Ltd.*, Version 1.171.37.35g.
- 19 O. V. Dolomanov, L. J. Bourhis, R. J. Gildea, J. A. K. Howard and H. Puschmann, *J. Appl. Crystallogr.*, 2009, **42**, 339.
- 20 G. M. Sheldrick, *Acta Cryst. A*, 2008, **64**, 112.
- 21 M. J. Frisch, G. W. Trucks, H. B. Schlegel, G. E. Scuseria, M. A. Robb, J. R. Cheeseman, G. Scalmani, V. Barone, B. Mennucci, G. A. Petersson, H. Nakatsuji, M. Caricato, X. Li, H. P. Hratchian, A. F. Izmaylov, J. Bloino, G. Zheng, J. L. Sonnenberg, M. Hada, M. Ehara, K. Toyota, R. Fukuda, J. Hasegawa, M. Ishida, T. Nakajima, Y. Honda, O. Kitao, H. Nakai, T. Vreven, J. A. Montgomery Jr., J. E. Peralta, F. Ogliaro, M. Bearpark, J. J. Heyd, E. Brothers, K. N. Kudin, V. N. Staroverov, R. Kobayashi, J. Normand, K. Raghavachari, A. Rendell, J. C. Burant, S. S. Iyengar, J. Tomasi, M. Cossi, N. Rega, J. M. Millam, M. Klene, J. E. Knox, J. B. Cross, V. Bakken, C. Adamo, J. Jaramillo, R. Gomperts, R. E. Stratmann, O. Yazyev, A. J. Austin, R. Cammi, C. Pomelli, J. W. Ochterski, R. L. Martin, K. Morokuma, V. G. Zakrzewski, G. A. Voth, P. Salvador, J. J. Dannenberg, S. Dapprich, A. D. Daniels, Ö. Farkas, J. B. Foresman, J. V. Ortiz, J. Cioslowski and D. J. Fox, *Gaussian, Inc.*, Wallingford CT, 2009.
- 22 J. Tomasi, B. Mennucci and R. Cammi, *Chem. Rev.*, 2005, **105**, 2999.
- 23 A. D. Becke, *J. Chem. Phys.*, 1993, **98**, 5648.
- 24 D. Paschoal, B. L. Marcial, J. Fedoce-Lopes, W. B. De Almeida and H. F. Dos Santos, *J. Comput. Chem.*, 2012, **33**, 2292.
- 25 B. Mennucci and J. Tomasi, *J. Chem. Phys.*, 1997, **106**, 5151.
- 26 M. T. Cancès, B. Mennucci and J. Tomasi, *J. Chem. Phys.*, 1997, **107**, 3032.
- 27 M. Cossi, V. Barone, B. Mennucci and J. Tomasi, *Chem. Phys. Lett.*, 1998, **286**, 253.
- 28 S. C. Dhara, *Indian J. Chem.*, 1970, **8**, 193.
- 29 L. Yang, D. R. Powell and R. P. Houser, *Dalton Trans.*, 2007, 955.
- 30 A. Okuniewski, D. Rosiak, J. Chojnacki and B. Becker, *Polyhedron*, 2015, **90**, 47.
- 31 A. S. Mahadevi and G. N. Sastry, *Chem. Rev.*, 2016, **116**, 2775.
- 32 R. Kruszynski and T. Sierański, *Cryst. Growth Des.*, 2016, **16**, 587.
- 33 M. A. Spackman and D. Jayatilaka, *CrystEngComm*, 2009, **11**, 19.
- 34 M. A. Spackman and J. J. McKinnon, *CrystEngComm*, 2002, **4**, 378.
- 35 S. K. Wolff, D. J. Grimwood, J. J. McKinnon, M. J. Turner, D. Jayatilaka and M. A. Spackman, *Crystal Explorer (Version 3.1)*, University of Western Australia, 2012.
- 36 N. M. O'Boyle, A. L. Tenderholt and K. M. Langner, *J. Comput. Chem.*, 2008, **29**, 839.
- 37 A. K. Pati, S. J. Gharpure and A. K. Mishra, *J. Phys. Chem. A*, 2015, **119**, 10481.
- 38 L. M. Hight, M. C. McGuire, Y. Zhang, M. A. Bork, P. E. Fanwick, A. Wasserman and D. R. McMillin, *Inorg. Chem.*, 2013, **52**, 8476.
- 39 F. Michalec, S. A. Bejune, D. G. Cuttell, G. C. Summerton, J. A. Gertenbach, J. S. Field, R. J. Haines and D. R. McMillin, *Inorg. Chem.*, 2001, **40**, 2193.
- 40 M. Utsuno, T. Yutaka, M. Murata, M. Kurihara, N. Tamai and H. Nishihara, *Inorg. Chem.*, 2007, **46**, 11291.
- 41 V. Karunakaran, D. D. Prabhu and S. Das, *J. Phys. Chem. C*, 2013, **117**, 9404.
- 42 A. Maroń, A. Szlapa, T. Klemens, S. Kula, B. Machura, S. Krompiec, J. G. Małecki, A. Świtlicka-Olszewska, K. Erfurt and A. Chrobok, *Org. Biomol. Chem.*, 2016, **14**, 3793.